

## Band Gap and Band Offset of $\text{Ga}_2\text{O}_3$ and $(\text{Al}_x\text{Ga}_{1-x})_2\text{O}_3$ Alloys

Tianshi Wang, Wei Li, Chaoying Ni, and Anderson Janotti\*

*Department of Materials Science and Engineering, University of Delaware, Newark, Delaware 19716, USA*



(Received 29 March 2018; revised manuscript received 26 June 2018; published 31 July 2018)

$\text{Ga}_2\text{O}_3$  and  $(\text{Al}_x\text{Ga}_{1-x})_2\text{O}_3$  alloys are promising materials for solar-blind UV photodetectors and high-power transistors. Basic key parameters in the device design, such as band-gap variation with alloy composition and band offset between  $\text{Ga}_2\text{O}_3$  and  $(\text{Al}_x\text{Ga}_{1-x})_2\text{O}_3$ , are yet to be established. Using density-functional theory with the Heyd-Scuseria-Ernzerhof hybrid functional, we compute formation enthalpies, band gaps, and band-edge positions of  $(\text{Al}_x\text{Ga}_{1-x})_2\text{O}_3$  alloys in the monoclinic ( $\beta$ ) and corundum ( $\alpha$ ) phases. We find the formation enthalpies of  $(\text{Al}_x\text{Ga}_{1-x})_2\text{O}_3$  alloys are significantly lower than of  $(\text{In}_x\text{Ga}_{1-x})_2\text{O}_3$ , and that  $(\text{Al}_x\text{Ga}_{1-x})_2\text{O}_3$  with  $x = 0.5$  can be considered as an ordered compound  $\text{AlGaO}_3$  in the monoclinic phase, with Al occupying the octahedral sites and Ga occupying the tetrahedral sites. The band gaps of the alloys range from 4.69 to 7.03 eV for  $\beta$ - $(\text{Al}_x\text{Ga}_{1-x})_2\text{O}_3$  and from 5.26 to 8.56 eV for  $\alpha$ - $(\text{Al}_x\text{Ga}_{1-x})_2\text{O}_3$ . Most of the band offset of the  $(\text{Al}_x\text{Ga}_{1-x})_2\text{O}_3$  alloy arises from the discontinuity in the conduction band. Our results are used to explain the available experimental data, and consequences for designing MODFETs based on  $(\text{Al}_x\text{Ga}_{1-x})_2\text{O}_3/\text{Ga}_2\text{O}_3$  are discussed.

DOI: 10.1103/PhysRevApplied.10.011003

$\text{Ga}_2\text{O}_3$  has been intensively investigated as a wide-band-gap semiconductor for high-power electronics [1–3] and UV solar-blind photodetectors [4,5]. It is available as large single crystals [6] suitable for high-quality epitaxial thin-film growth by metalorganic chemical vapor deposition (MOCVD) [7,8] and molecular beam epitaxy (MBE) [5,9]; it displays high breakdown electric field [1], and the Baliga figure of merit exceeds that of SiC and GaN [3]; it can be easily doped *n*-type, and band-gap engineering can be accomplished by incorporating In and Al, adding great flexibility to device design. Modulation doping of  $(\text{Al}_x\text{Ga}_{1-x})_2\text{O}_3/\text{Ga}_2\text{O}_3$  heterostructures can be used to separate the ionized donors in the  $(\text{Al}_x\text{Ga}_{1-x})_2\text{O}_3$  layer from the conduction electrons in the  $\text{Ga}_2\text{O}_3$  layer [10–13], providing a boost to the electron mobility to about  $500 \text{ cm}^2 \text{ V}^{-1} \text{ s}^{-1}$  [10,14,15] by suppressing scattering from the ionized impurities. Simulated band diagrams and a 2DEG profile of MODFETs based on  $(\text{Al}_x\text{Ga}_{1-x})_2\text{O}_3/\text{Ga}_2\text{O}_3$  assumed that the discontinuity in the band offset appears solely on the conduction band [10]. However, this assumption has not been based on firm experimental evidence or first-principles calculations. The band gap of the  $(\text{Al}_x\text{Ga}_{1-x})_2\text{O}_3$  alloy and the band offset between the  $(\text{Al}_x\text{Ga}_{1-x})_2\text{O}_3$  and  $\text{Ga}_2\text{O}_3$  are key parameters in the device design and are yet to be established.

$\text{Ga}_2\text{O}_3$  and  $(\text{Al}_x\text{Ga}_{1-x})_2\text{O}_3$  can be made in the monoclinic ( $\beta$ ) and in the corundum ( $\alpha$ ) phase, as shown

in Fig. 1. Bulk and thin films of  $\beta$ - $(\text{Al}_x\text{Ga}_{1-x})_2\text{O}_3$  have been obtained using solution combustion synthesis [16], pulsed laser deposition (PLD) [17], and oxygen plasma-assisted MBE [10–12], while  $\alpha$ - $(\text{Al}_x\text{Ga}_{1-x})_2\text{O}_3$  have been grown on sapphire substrates by CVD for Al content of up to 81% [18,19]. Band gaps of  $(\text{Al}_x\text{Ga}_{1-x})_2\text{O}_3$  for selected Al content have been reported [16–20], but band offsets between  $\text{Ga}_2\text{O}_3$  and  $(\text{Al}_x\text{Ga}_{1-x})_2\text{O}_3$ , which are much more challenging to obtain experimentally, are still unknown.

Using density functional theory (DFT) and the Heyd-Scuseria-Ernzerhof (HSE) hybrid functional, we investigate the formability of  $(\text{Al}_x\text{Ga}_{1-x})_2\text{O}_3$  alloys in both  $\beta$  and  $\alpha$  phases, their band gaps as a function of Al concentration, and the band offsets of the  $(\text{Al}_x\text{Ga}_{1-x})_2\text{O}_3$  alloys with respect to  $\text{Ga}_2\text{O}_3$  and  $\text{Al}_2\text{O}_3$ . In the following, we first describe the details of the calculations, present the results for structural parameters and stability of the alloys, and then discuss the results for band gaps and band offsets for both  $\beta$  and  $\alpha$  phases and the implications for device design.

The calculations are based on DFT [33,34] with the projector augmented wave (PAW) method [35] as implemented in the VASP code [36,37]. The *d* states of Ga are included as valence states, and a plane-wave cutoff energy of 400 eV is employed. We use the Perdew-Burke-Ernzerhof functional revised for solids (PBEsol) [38] to relax all structures. To overcome the severe underestimation of band gaps in the DFT PBEsol functional, we employ the screened hybrid functional of Heyd, Scuseria, and Ernzerhof (HSE06) [39,40]. In the HSE hybrid

\*janotti@udel.edu

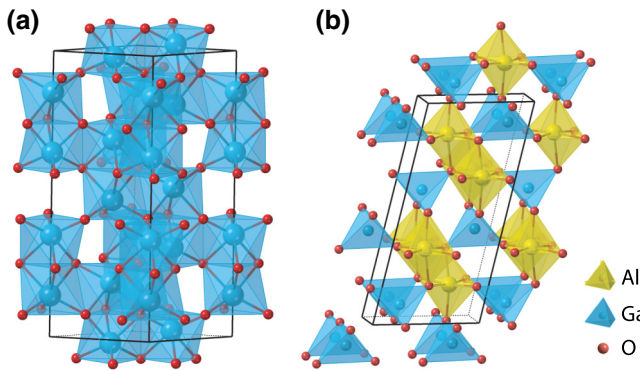


FIG. 1. Conventional unit cells of (a)  $\alpha$ - $\text{Ga}_2\text{O}_3$  and (b)  $\beta$ - $\text{AlGaO}_3$  compounds. In the latter, the Al atoms occupy octahedral sites and Ga occupy tetrahedral sites, maintaining the same structure as its parent compounds  $\beta$ - $\text{Ga}_2\text{O}_3$  and  $\theta$ - $\text{Al}_2\text{O}_3$ .

functional, the nonlocal Hartree-Fock exchange is mixed with the generalized gradient approximation (GGA) [41] exchange in the short-range part. The mixing parameter in HSE is fixed to 32% for all the calculations. We find that this choice of mixing parameter gives band gaps of the parent compounds  $\text{Ga}_2\text{O}_3$  and  $\text{Al}_2\text{O}_3$  in good agreement with experimental values. Note that, conventionally, monoclinic  $\text{Al}_2\text{O}_3$  is often denoted as the  $\theta$  phase in the literature, i.e.,  $\theta$ - $\text{Al}_2\text{O}_3$  shares the same crystal structure as  $\beta$ - $\text{Ga}_2\text{O}_3$  [21–23]. The calculated lattice parameters, formation enthalpies, and band gaps for  $\text{Al}_2\text{O}_3$  and  $\text{Ga}_2\text{O}_3$  are listed in Table I along with the available experimental

data. The  $\theta$ - $\text{Al}_2\text{O}_3$ ,  $\alpha$ - $\text{Ga}_2\text{O}_3$ , and  $\beta$ - $\text{Ga}_2\text{O}_3$  have indirect gaps where the valence-band maximum is higher than the valence-band edge at  $\Gamma$  by 0.16, 0.24, and 0.04 eV, respectively, as previously reported [42].

We simulate  $(\text{Al}_x\text{Ga}_{1-x})_2\text{O}_3$  random alloys using special quasirandom structures (SQS) [43] generated using the mcsqs code of the Alloy Theoretic Automated Toolkit (ATAT) [44]. This method can generate optimal periodic supercells comparable to true disordered structures based on a Monte Carlo simulated annealing loop with an objective function that seeks to perfectly match the maximum number of correlation functions [44].

We use supercells containing 80 atoms for the  $\alpha$  and 120 atoms for the  $\beta$  phase. In the case of  $\alpha$ - $\text{Ga}_2\text{O}_3$ , all Ga sites are equivalent; therefore, Al tends to replace Ga randomly. However, in the case of  $\beta$ - $\text{Ga}_2\text{O}_3$ , half of the Ga atoms are at octahedral sites and the other half at tetrahedral sites. We find that Al strongly prefers octahedral sites, i.e., Al sitting at octahedral sites is approximately 0.2 eV per Al atom lower in energy than Al sitting at tetrahedral sites. Therefore, in the generation of SQS structures to simulate  $\beta$ - $(\text{Al}_x\text{Ga}_{1-x})_2\text{O}_3$  alloys, we assumed that Al atoms occupy only octahedral sites for  $x \leq 0.5$ . For  $x > 0.5$ , Al atoms exceeding  $x > 0.5$  randomly replace Ga at tetrahedral sites since all octahedral sites are already filled.

Figure 2 shows the calculated equilibrium volume of  $(\text{Al}_x\text{Ga}_{1-x})_2\text{O}_3$  alloys as a function of Al fraction. For  $\alpha$ - $(\text{Al}_x\text{Ga}_{1-x})_2\text{O}_3$ , the volume varies linearly with Al composition, following Vegard's law. For  $\beta$ - $(\text{Al}_x\text{Ga}_{1-x})_2\text{O}_3$ , the volume also decreases monotonically with Al fraction, but

TABLE I. Calculated lattice parameters, formation enthalpy ( $\Delta H$ ), and band gaps ( $E_g$ ) of  $\text{Al}_2\text{O}_3$  and  $\text{Ga}_2\text{O}_3$  in corundum ( $\alpha$ - $\text{Al}_2\text{O}_3$  and  $\alpha$ - $\text{Ga}_2\text{O}_3$ ) and monoclinic ( $\theta$ - $\text{Al}_2\text{O}_3$  and  $\beta$ - $\text{Ga}_2\text{O}_3$ ) structures. The indirect and direct band gaps are denoted as (i) and (d), respectively. Note that monoclinic  $\text{Al}_2\text{O}_3$  is often denoted as the  $\theta$  phase in the literature, i.e.,  $\theta$ - $\text{Al}_2\text{O}_3$  shares the same crystal structure as  $\beta$ - $\text{Ga}_2\text{O}_3$  [21–23].

	$\alpha$ - $\text{Al}_2\text{O}_3$		$\theta$ - $\text{Al}_2\text{O}_3$		$\alpha$ - $\text{Ga}_2\text{O}_3$		$\beta$ - $\text{Ga}_2\text{O}_3$	
	Calc.	Expt.	Calc.	Expt.	Calc.	Expt.	Calc.	Expt.
$a$ (Å)	4.774	4.76 <sup>a</sup>	11.808	11.795 <sup>b</sup>	5.005	4.983 <sup>c</sup>	12.276	12.214 <sup>d</sup>
$b$ (Å)			2.921	2.910 <sup>b</sup>			3.050	3.037 <sup>d</sup>
$c$ (Å)	13.013	12.99 <sup>a</sup>	5.636	5.621 <sup>b</sup>	13.454	13.433 <sup>c</sup>	5.811	5.798 <sup>d</sup>
$\beta$ (deg)			104.08	103.79 <sup>b</sup>			103.72	103.83
$\Delta H$ (eV/f.u.)	-15.753	-16.971 <sup>e</sup>	-15.561		-9.824		-9.870	-11.30 <sup>f</sup>
$E_g$ (eV)	8.56 (d)	8.8 <sup>g</sup>	7.03 (i)		5.26 (i)	5.3 <sup>h</sup>	4.69 (i)	4.48 <sup>i</sup> , 4.9 <sup>j</sup>

<sup>a</sup>Ref. [24].

<sup>b</sup>Ref. [23].

<sup>c</sup>Ref. [25].

<sup>d</sup>Ref. [26].

<sup>e</sup>Ref. [27].

<sup>f</sup>Ref. [28].

<sup>g</sup>Ref. [29].

<sup>h</sup>Ref. [30].

<sup>i</sup>Ref. [31].

<sup>j</sup>Ref. [32].

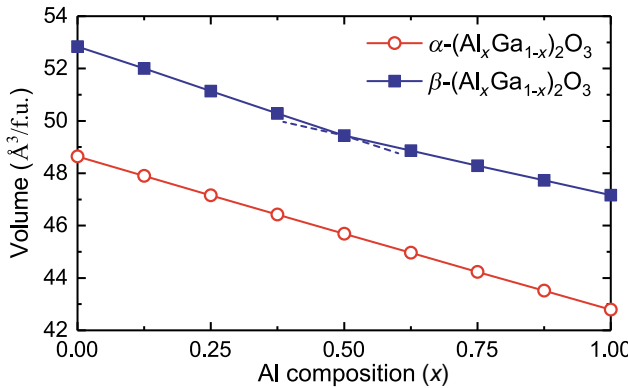


FIG. 2. Calculated equilibrium volume of  $\alpha$  and  $\beta$ - $(\text{Al}_x\text{Ga}_{1-x})_2\text{O}_3$  alloys as a function of Al concentration ( $x$ ).

exhibits a change in slope at  $x = 0.5$ . This discontinuity in the slope is attributed to Al occupying the tetrahedral sites for  $x > 0.5$ . This trend was recently observed by Krueger et al. [16].

The calculated formation enthalpies of  $\text{Ga}_2\text{O}_3$  and  $\text{Al}_2\text{O}_3$ , defined as the total energy of the compound minus the total energies of the elemental bulk phases, are listed in Table I. We find that the formation enthalpy of  $\alpha$ - $\text{Ga}_2\text{O}_3$  is only 46 meV/f.u. higher than  $\beta$ - $\text{Ga}_2\text{O}_3$ . In contrast,  $\alpha$ - $\text{Al}_2\text{O}_3$  is much more stable than  $\theta$ - $\text{Al}_2\text{O}_3$ , by 192 meV/f.u. This is again attributed to the preference of Al occupying octahedral sites, by  $\sim 0.2$  eV per cation. Figures 3(a) and 3(b) show the formation enthalpies of  $\alpha$  and  $\beta$ - $(\text{Al}_x\text{Ga}_{1-x})_2\text{O}_3$ , defined as

$$\Delta H[(\text{Al}_x\text{Ga}_{1-x})_2\text{O}_3] = E[(\text{Al}_x\text{Ga}_{1-x})_2\text{O}_3] - xE[\text{Al}_2\text{O}_3] - (1-x)E[\text{Ga}_2\text{O}_3], \quad (1)$$

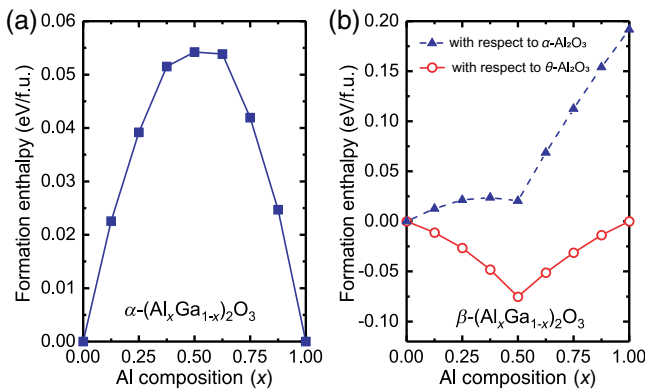


FIG. 3. Formation enthalpies of (a)  $\alpha$  and (b)  $\beta$ - $(\text{Al}_x\text{Ga}_{1-x})_2\text{O}_3$  with respect to the parent compounds  $\text{Ga}_2\text{O}_3$  and  $\text{Al}_2\text{O}_3$ . For  $\beta$ - $(\text{Al}_x\text{Ga}_{1-x})_2\text{O}_3$ , formation enthalpies calculated with respect to  $\beta$ - $\text{Ga}_2\text{O}_3 + \theta$ - $\text{Al}_2\text{O}_3$  (red circles) and  $\beta$ - $\text{Ga}_2\text{O}_3 + \alpha$ - $\text{Al}_2\text{O}_3$  (blue triangles) are shown.

where  $E[(\text{Al}_x\text{Ga}_{1-x})_2\text{O}_3]$  is the total energy of the SQS supercell structure representing the random alloy, and  $E[\text{Ga}_2\text{O}_3]$  and  $E[\text{Al}_2\text{O}_3]$  are the total energies of the parent compounds  $\text{Ga}_2\text{O}_3$  and  $\text{Al}_2\text{O}_3$  in the same supercell. The formation enthalpies of  $\alpha$ - $(\text{Al}_x\text{Ga}_{1-x})_2\text{O}_3$  are relatively small compared to other alloys. For example, at  $x = 0.5$ , the formation enthalpy of  $\alpha$ - $(\text{In}_x\text{Ga}_{1-x})_2\text{O}_3$  is approximately 300 meV/f.u. [45], compared to 55 meV/f.u. for  $(\text{Al}_x\text{Ga}_{1-x})_2\text{O}_3$ . This indicates that  $\alpha$ - $(\text{Al}_x\text{Ga}_{1-x})_2\text{O}_3$  alloys are more likely to form at all Al compositions. In the case of  $\beta$ - $(\text{Al}_x\text{Ga}_{1-x})_2\text{O}_3$ , we find a stable ordered compound  $\text{AlGaO}_3$  for 50% Al content. If taken with respect to  $\alpha$ - $\text{Al}_2\text{O}_3$  (dashed line), which is the most stable phase of  $\text{Al}_2\text{O}_3$ , the formation enthalpy of  $\beta$ - $(\text{Al}_x\text{Ga}_{1-x})_2\text{O}_3$  rapidly increases with Al composition above 50%. Again, this is explained by the fact that Al strongly prefer to occupy the octahedral sites for  $x \leq 0.5$ , but end up occupying the only available tetrahedral sites for  $x > 0.5$ .

Therefore, for Al concentrations approaching 100%, we predict that  $(\text{Al}_x\text{Ga}_{1-x})_2\text{O}_3$  alloys strongly favor the corundum or  $\alpha$  phase. This explains why the single monoclinic phase at  $0 \leq x < 0.8$  and mixed corundum and monoclinic phases for  $0.8 \leq x < 1$  have been observed by solution combustion synthesis [16]. We note, however, that thin films of  $\beta$ - $(\text{Al}_x\text{Ga}_{1-x})_2\text{O}_3$  alloys with Al content up to 96% have been reported using PLD [17].

The calculated band gap of  $(\text{Al}_x\text{Ga}_{1-x})_2\text{O}_3$  alloys as a function of Al content is shown in Fig. 4. The band-gap bowing parameter  $b$  is derived by fitting the results using

$$E_g[(\text{Al}_x\text{Ga}_{1-x})_2\text{O}_3] = (1-x)E_g[\text{Ga}_2\text{O}_3] + xE_g[\text{Al}_2\text{O}_3] - bx(1-x). \quad (2)$$

We obtain a bowing parameter of 1.6 eV for  $\alpha$  and 1.0 eV for the  $\beta$ - $(\text{Al}_x\text{Ga}_{1-x})_2\text{O}_3$  alloys. Overall, our results are in good agreement with the available experimental data [16–20], also shown in Fig. 4. Due to the stability of the ordered  $\text{AlGaO}_3$  ( $x = 0.5$ ), we can define two independent bowing parameters, one for  $0 \leq x \leq 0.5$  and another for  $0.5 \leq x \leq 1$ . These are listed in the Supplemental Material along the bowing parameters for the VBM and conduction-band minimum (CBM) separately [46].

The band offsets between  $(\text{Al}_x\text{Ga}_{1-x})_2\text{O}_3$  and the parent compound  $\text{Ga}_2\text{O}_3$  are crucial parameters in the design of electronic devices that depend on carrier confinement or on the separation between carriers and ionized impurities such as in MODFETs [10,15]. We calculated the band offset between two materials using the following procedure [47]. First, the VBM and the CBM of the bulk materials are determined with respect to the averaged electrostatic potential. Then, we align the averaged electrostatic potential in the two materials by performing an interface calculation. In this case, we used supercells composed of 12 layers of each material with two equivalent interfaces. The supercells are constructed along nonpolar directions to avoid

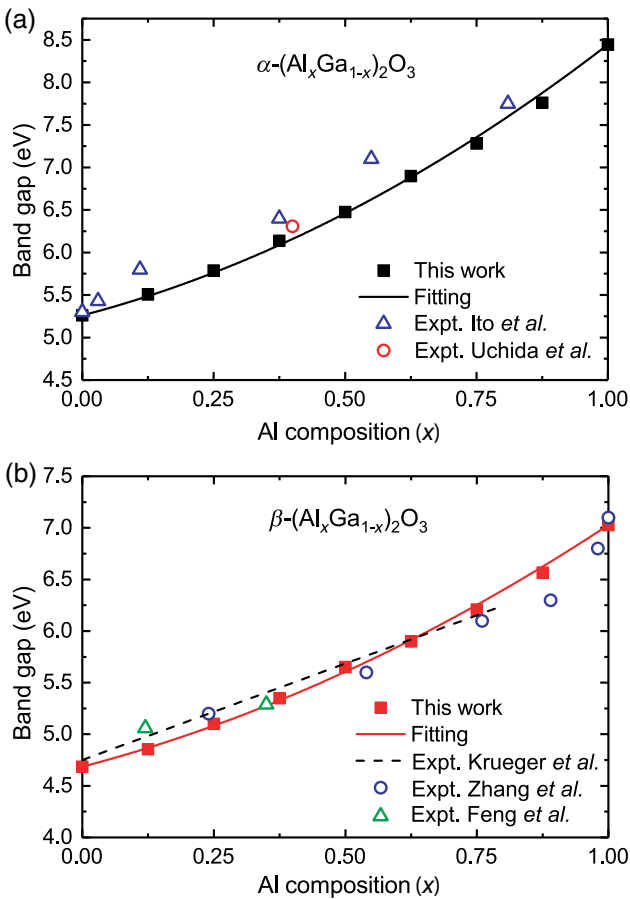


FIG. 4. Band gaps of (a)  $\alpha$  and (b)  $\beta$ - $(\text{Al}_x\text{Ga}_{1-x})_2\text{O}_3$  as a function of Al fraction  $x$ . As shown, the calculated results (solid squares) are fitted as solid lines using Eq. (2). The experimental results are from the onset of photoemission inelastic losses in x-ray photoelectron spectroscopy [16], transmittance and x-ray photoelectron spectroscopy [17], energy-loss spectra [19], and optical transmittance and optical absorption spectra [18,20].

problems resulting from the polar discontinuity at the interface and the consequent slopes in the averaged electrostatic potential in the bulk regions. For  $\text{Ga}_2\text{O}_3$  and  $\text{Al}_2\text{O}_3$  in the monoclinic phase, we chose a superlattice geometry along the [010] nonpolar direction. For the corundum phase, we constructed a superlattice along the [100] nonpolar direction. To avoid the problem of lattice mismatch, we used average in-plane lattice parameters; the out-of-plane lattice parameter is set so that each material in the superlattice has its equilibrium volume. In this way, the averaged electrostatic potentials in each side of the interface correspond to the average electrostatic potential in the respective bulk materials. This procedure, therefore, gives us the natural band offset between  $\text{Ga}_2\text{O}_3$  and  $\text{Al}_2\text{O}_3$ .

For monoclinic  $\text{Ga}_2\text{O}_3$  and  $\text{Al}_2\text{O}_3$ , we find a type II staggered alignment, with a valence-band offset of 0.33 eV and a conduction-band offset of 2.67 eV, as shown in Fig. 5(a).

Thus, 89% of the band offset arises from the discontinuity in the conduction band, and only 11% comes from the valence band. In the case of corundum  $\text{Ga}_2\text{O}_3$  and  $\text{Al}_2\text{O}_3$ , we find a type I straddling alignment, with 0.11 eV valence-band offset and 3.19 eV conduction-band offset, also shown in Fig. 5(a), i.e., 97% of the offset comes from the conduction band, and only 3% from the valence band.

We also determined the absolute position of the valence and conduction bands by taking the averaged electrostatic potential of  $\alpha$  and  $\beta$ - $\text{Ga}_2\text{O}_3$  with respect to the vacuum level using surface calculations of nonpolar terminations. The results are shown in the energy axis of Fig. 5(a), where we also added the band-edge positions of amorphous  $\text{Al}_2\text{O}_3$  according to previous experimental results of band gap and valence-band offset with  $\alpha$ - $\text{Al}_2\text{O}_3$  from Ref. [48] for comparison.

Finally, we determined the band-edge positions in  $(\text{Al}_x\text{Ga}_{1-x})_2\text{O}_3$  with respect to that in  $\text{Ga}_2\text{O}_3$  and  $\text{Al}_2\text{O}_3$ . The averaged electrostatic potential for a given alloy composition is derived from a linear interpolation of the averaged electrostatic potential of the constituent compounds. Figures 5(b) and 5(c) show the derived VBM and CBM positions for  $\alpha$  and  $\beta$ - $(\text{Al}_x\text{Ga}_{1-x})_2\text{O}_3$  as a function of Al composition. The valence-band edges only change slightly with Al concentration  $x$ , while most of the change occurs in the CBM. This is expected since O 2p states dominate the VBM. All the band gap values, the absolute position of VBM and CBM, and the corresponding bowing parameters are listed in the Supplemental Material [46].

The results above have important implications to device design. For instance, for Al concentration of 20% we find that the conduction-band offset between monoclinic  $(\text{Al}_{0.2}\text{Ga}_{0.8})_2\text{O}_3$  and  $\text{Ga}_2\text{O}_3$  of 0.47 eV, compared to the assumed 0.6 eV in Ref. [10] for a MODFET structure. This relatively small conduction-band offset for 20% Al content in the alloy can be insufficient so that electrons from the 2DEG at the  $(\text{Al}_{0.2}\text{Ga}_{0.8})_2\text{O}_3/\text{Ga}_2\text{O}_3$  may stay in the Si  $\delta$ -doped layer in the  $(\text{Al}_{0.2}\text{Ga}_{0.8})_2\text{O}_3$  alloy, causing a parasitic parallel channel of conduction in the MODFET [10]. Higher Al concentrations in the  $(\text{Al}_x\text{Ga}_{1-x})_2\text{O}_3$  film ( $\text{Al}_x\text{Ga}_{1-x}$ ) $_2\text{O}_3$ , resulting in increased conduction-band offsets, are required to overcome this detrimental effect.

We also note the discontinuity in the first-order derivative for the CBM and VBM at  $x = 0.5$  for  $\beta$ - $(\text{Al}_x\text{Ga}_{1-x})_2\text{O}_3$ . Like the discontinuities in volume and formation enthalpies, this is attributed to Al also occupying tetrahedral sites for  $x > 0.5$ . The kinks at  $x = 0.5$  in the equilibrium volume, formation enthalpies, and band-edge positions of  $(\text{Al}_x\text{Ga}_{1-x})_2\text{O}_3$  indicate that  $\beta$ - $\text{AlGaO}_3$  may well be considered an ordered compound with Al in octahedral sites and Ga in tetrahedral sites instead of a random alloy.

In summary, we find that  $(\text{Al}_x\text{Ga}_{1-x})_2\text{O}_3$  alloys have much lower mixing enthalpies than  $(\text{In}_x\text{Ga}_{1-x})_2\text{O}_3$ . The

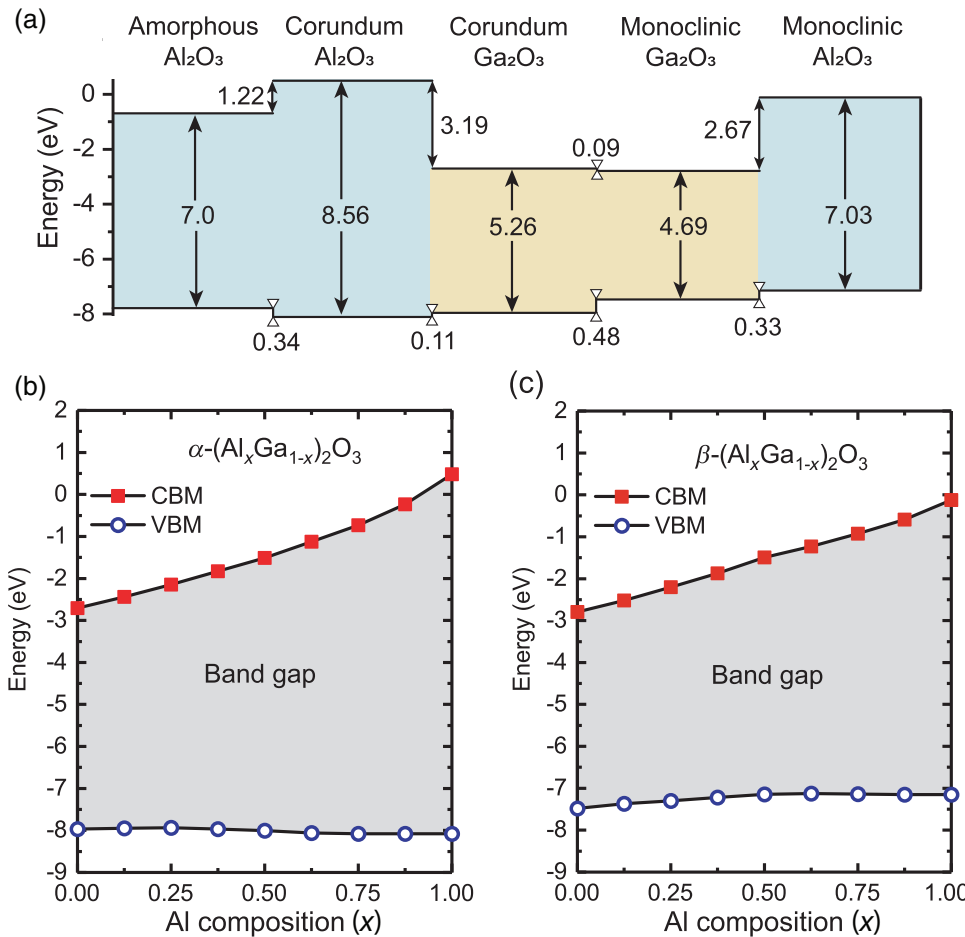


FIG. 5. (a) Calculated band offsets between  $\text{Ga}_2\text{O}_3$  and  $\text{Al}_2\text{O}_3$ . CBM and VBM positions of (c)  $\alpha$  and (d)  $\beta$ - $(\text{Al}_x\text{Ga}_{1-x})_2\text{O}_3$ . The zero in the energy axes corresponds to the vacuum level, determined as described in the text.

band gap of the alloys can be tuned in a wide range by changing Al composition, adding great flexibility in the design of  $(\text{Al}_x\text{Ga}_{1-x})_2\text{O}_3/\text{Ga}_2\text{O}_3$ -based electronic devices. The conduction-band discontinuity comprises 89% of the band offset between monoclinic  $\text{Al}_2\text{O}_3$  and  $\text{Ga}_2\text{O}_3$ , and 97% in the case of the corundum phase. Our results suggest that films with Al concentrations larger than 20% are required to avoid unwanted parallel conduction channel in MODFETs based on monoclinic  $(\text{Al}_x\text{Ga}_{1-x})_2\text{O}_3/\text{Ga}_2\text{O}_3$  heterostructures.

## ACKNOWLEDGMENTS

T.W. and C.N. are supported by the II-VI Foundation, and A.J. is supported by the National Science Foundation Grant No. DMR-1652994. This research is supported through the use of the Extreme Science and Engineering Discovery Environment (XSEDE) supercomputer facility, National Science Foundation Grant No. ACI-1053575, and the Information Technologies (IT) resources at the University of Delaware, specifically the high-performance computing resources.

- [1] Masataka Higashiwaki, Kohei Sasaki, Akito Kuramata, Takekazu Masui, and Shigenobu Yamakoshi, Gallium oxide ( $\text{Ga}_2\text{O}_3$ ) metal-semiconductor field-effect transistors on single-crystal  $\beta$ - $\text{Ga}_2\text{O}_3$  (010) substrates, *Appl. Phys. Lett.* **100**, 013504 (2012).
- [2] Higashiwaki Masataka, Sasaki Kohei, Murakami Hisashi, Kumagai Yoshinao, Koukitu Akinori, Kuramata Akito, Masui Takekazu, and Yamakoshi Shigenobu, Recent progress in  $\text{Ga}_2\text{O}_3$  power devices, *Semicond. Sci. Technol.* **31**, 34001 (2016).
- [3] G. Jessen, K. Chabak, A. Green, J. McCandless, S. Tetlak, K. Leedy, R. Fitch, S. Mou, E. Heller, S. Badescu, A. Crespo, and N. Moser, in Device Res. Conf., Vol. 75th Annual (2017), pp. 1–2.
- [4] Takayoshi Oshima, Takeya Okuno, Naoki Arai, Norihito Suzuki, Shigeo Ohira, and Shizuo Fujita, Vertical solar-blind deep-ultraviolet schottky photodetectors based on  $\beta$ - $\text{Ga}_2\text{O}_3$  substrates, *Appl. Phys. Express* **1**, 011202 (2008).
- [5] Takayoshi Oshima, Takeya Okuno, and Shizuo Fujita,  $\text{Ga}_2\text{O}_3$  thin film growth on *c*-plane sapphire substrates by molecular beam epitaxy for deep-ultraviolet photodetectors, *Jpn. J. Appl. Physics* **46**, 7217 (2007).

- [6] Hideo Aida, Kengo Nishiguchi, Hidetoshi Takeda, Natsuko Aota, Kazuhiko Sunakawa, and Yoichi Yaguchi, Growth of  $\beta$ -Ga<sub>2</sub>O<sub>3</sub> single crystals by the edge-defined, film fed growth method, *Jpn. J. Appl. Phys.* **47**, 8506 (2008).
- [7] Xuejian Du, Zhao Li, Caina Luan, Weiguang Wang, Mingxian Wang, Xianjin Feng, Hongdi Xiao, and Jin Ma, Preparation and characterization of Sn-doped  $\beta$ -Ga<sub>2</sub>O<sub>3</sub> homoepitaxial films by MOCVD, *J. Mater. Sci.* **50**, 3252 (2015).
- [8] Michele Baldini, Martin Albrecht, Andreas Fiedler, Klaus Irmischer, Robert Schewski, and Günter Wagner, Editors choice: Si- and Sn-doped homoepitaxial  $\beta$ -Ga<sub>2</sub>O<sub>3</sub> layers grown by MOVPE on (010)-oriented substrates, *ECS J. Solid State Sci. Technol.* **6**, Q3040 (2017).
- [9] Encarnación G. Villora, Kiyoshi Shimamura, Kenji Kitamura, and Kazuo Aoki, Rf-plasma-assisted molecular-beam epitaxy of  $\beta$ -Ga<sub>2</sub>O<sub>3</sub>, *Appl. Phys. Lett.* **88**, 031105 (2006).
- [10] Sriram Krishnamoorthy, Zhanbo Xia, Chandan Joishi, Yuewei Zhang, Joe McGlone, Jared Johnson, Aaron R. Arehart, Jinwoo Hwang, Saurabh Lodha, Siddharth Rajan, Sriram Krishnamoorthy, Zhanbo Xia, Chandan Joishi, Yuewei Zhang, Saurabh Lodha, and Siddharth Rajan, Modulation-doped  $\beta$ -(Al<sub>0.2</sub>Ga<sub>0.8</sub>)<sub>2</sub>O<sub>3</sub>/Ga<sub>2</sub>O<sub>3</sub> field-effect transistor, *Appl. Phys. Lett.* **111**, 023502 (2017).
- [11] Takayoshi Oshima, Yuji Kato, Naoto Kawano, Akito Kuramata, Shigenobu Yamakoshi, Shizuo Fujita, Toshiyuki Oishi, and Makoto Kasu, Carrier confinement observed at modulation-doped  $\beta$ -(Al<sub>x</sub>Ga<sub>1-x</sub>)<sub>2</sub>O<sub>3</sub>/Ga<sub>2</sub>O<sub>3</sub> heterojunction interface, *Appl. Phys. Express* **10**, 035701 (2017).
- [12] Elaheh Ahmadi, Onur S. Koksalidi, Xun Zheng, Tom Mates, Yuichi Oshima, Umesh K. Mishra, and James S. Speck, Demonstration of  $\beta$ -(Al<sub>x</sub>Ga<sub>1-x</sub>)<sub>2</sub>O<sub>3</sub>/ $\beta$ -Ga<sub>2</sub>O<sub>3</sub> modulation doped field-effect transistors with Ge as dopant grown via plasma-assisted molecular beam epitaxy, *Appl. Phys. Express* **10**, 071101 (2017).
- [13] Youngho Kang, Karthik Krishnaswamy, Hartwin Peelaers, and Chris G. Van de Walle, Fundamental limits on the electron mobility of  $\beta$ -Ga<sub>2</sub>O<sub>3</sub>, *J. Phys. Condens. Matter* **29**, 234001 (2017).
- [14] Nan Ma, Nicholas Tanen, Amit Verma, Zhi Guo, Tengfei Luo, Huili (Grace) Xing, and Debdeep Jena, Intrinsic electron mobility limits in  $\beta$ -Ga<sub>2</sub>O<sub>3</sub>, *Appl. Phys. Lett.* **109**, 212101 (2016).
- [15] Yuewei Zhang, Adam Neal, Zhanbo Xia, Chandan Joishi, Yuanhua Zheng, Sanyam Bajaj, Mark Brenner, Shin Mou, Donald Dorsey, Kelson Chabak, Gregg Jessen, Jinwoo Hwang, Joseph Heremans, and Siddharth Rajan, High mobility two-dimensional electron gas in modulation-doped  $\beta$ -(Al<sub>x</sub>Ga<sub>1-x</sub>)<sub>2</sub>O<sub>3</sub>/Ga<sub>2</sub>O<sub>3</sub> heterostructures, *Appl. Phys. Lett.* **112**, 173502 (2018).
- [16] Benjamin W. Krueger, Christopher S. Dandeneau, Evan M. Nelson, Scott T. Dunham, Fumio S. Ohuchi, and Marjorie A. Olmstead, Variation of band gap and lattice parameters of  $\beta$ -(Al<sub>x</sub>Ga<sub>1-x</sub>)<sub>2</sub>O<sub>3</sub> powder produced by solution combustion synthesis, *J. Am. Ceram. Soc.* **99**, 2467 (2016).
- [17] Fabi Zhang, Katsuhiko Saito, Tooru Tanaka, Mitsuhiro Nishio, Makoto Arita, and Qixin Guo, Wide bandgap engineering of (AlGa)<sub>2</sub>O<sub>3</sub> films, *Appl. Phys. Lett.* **105**, 162107 (2014).
- [18] Hiroshi Ito, Kentaro Kaneko, and Shizuo Fujita, Growth and band gap control of corundum-structured  $\alpha$ -(AlGa)<sub>2</sub>O<sub>3</sub> thin films on sapphire by spray-assisted mist chemical vapor deposition, *Jpn. J. Appl. Phys.* **51**, 100207 (2012).
- [19] T. Uchida, R. Jinno, S. Takemoto, K. Kaneko, and S. Fujita, in *2016 Compound Semiconductor Week (CSW) [Includes 28th International Conference on Indium Phosphide & Related Materials (IPRM) & 43rd International Symposium on Compound Semiconductors (ISCS)]* (Toyama, 2016) pp. 1–2.
- [20] Qian Feng, Xiang Li, Genquan Han, Lu Huang, Fuguo Li, Weihua Tang, Jincheng Zhang, and Yue Hao, (AlGa)<sub>2</sub>O<sub>3</sub> solar-blind photodetectors on sapphire with wider bandgap and improved responsivity, *Opt. Mater. Express* **7**, 1240 (2017).
- [21] Yamaguchi Goro, Yasui Itaru, and Wen-Chau Chiu, A new method of preparing theta-alumina and the interpretation of its x-ray power diffraction pattern and electron diffraction pattern, *Bull. Chem. Soc. Japan* **43**, 2487 (1970).
- [22] Rong-Sheng Zhou and Robert L. Snyder, Structures and transformation mechanisms of the  $\eta$ ,  $\gamma$  and  $\theta$  transition aluminas, *Acta Crystallogr. B* **47**, 617 (1991).
- [23] E. Husson and Y. Repelin, Structural studies of transition aluminas. Theta alumina, *Eur. J. Solid State Inorg. Chem.* **33**, 1223 (1996).
- [24] E. E. Newnham and Y. M. DeHaan, Refinement of the  $\alpha$  Al<sub>2</sub>O<sub>3</sub>, Ti<sub>2</sub>O<sub>3</sub>, V<sub>2</sub>O<sub>3</sub> and Cr<sub>2</sub>O<sub>3</sub> structures, *Zeitschrift für Krist. Mater.* **117**, 235 (1962).
- [25] M. Marezio and J. P. Remeika, Bond lengths in the  $\alpha$ -Ga<sub>2</sub>O<sub>3</sub> structure and the high-pressure phase of Ga<sub>2-x</sub>Fe<sub>x</sub>O<sub>3</sub>, *J. Chem. Phys.* **46**, 1862 (1967).
- [26] John Åhman, Göran Svensson, and Jörgen Albertsson, A reinvestigation of  $\beta$ -gallium oxide, *Acta Crystallogr.* **52**, 1336 (1996).
- [27] D. Ghosh and D. A. R. Kay, Standard free energy of formation of alumina, *J. Electrochem. Soc.* **124**, 1836 (1977).
- [28] İhsan Barin, in *Thermochem. Data Pure Subst.* (Wiley-VCH Verlag GmbH, 2008), pp. 728–780.
- [29] Roger H. French, Electronic band structure of Al<sub>2</sub>O<sub>3</sub>, with comparison to Alon and AlN, *J. Am. Ceram. Soc.* **73**, 477 (1990).
- [30] Daisuke Shinohara and Shizuo Fujita, Heteroepitaxy of corundum-structured  $\alpha$ -Ga<sub>2</sub>O<sub>3</sub> thin films on  $\alpha$ -Al<sub>2</sub>O<sub>3</sub> substrates by ultrasonic mist chemical vapor deposition, *Jpn. J. Appl. Phys.* **47**, 7311 (2008).
- [31] Takeyoshi Onuma, Shingo Saito, Kohei Sasaki, Tatekazu Masui, Tomohiro Yamaguchi, Tohru Honda, and Masataka Higashiwaki, Valence band ordering in  $\beta$ -Ga<sub>2</sub>O<sub>3</sub> studied by polarized transmittance and reflectance spectroscopy, *Jpn. J. Appl. Phys.* **54**, 112601 (2015).
- [32] Masahiro Orita, Hiromichi Ohta, Masahiro Hirano, and Hideo Hosono, Deep-ultraviolet transparent conductive  $\beta$ -Ga<sub>2</sub>O<sub>3</sub> thin films, *Appl. Phys. Lett.* **77**, 4166 (2000).
- [33] P. Hohenberg and W. Kohn, Inhomogeneous electron gas, *Phys. Rev.* **136**, B864 (1964).
- [34] W. Kohn and L. J. Sham, Self-consistent equations including exchange and correlation effects, *Phys. Rev.* **140**, A1133 (1965).

- [35] P. E. Blöchl, Projector augmented-wave method, *Phys. Rev. B* **50**, 17953 (1994).
- [36] G. Kresse and J. Hafner, *Ab initio* molecular dynamics for liquid metals, *Phys. Rev. B* **47**, 558 (1993).
- [37] G. Kresse and J. Hafner, *Ab initio* molecular-dynamics simulation of the liquid-metal–amorphous-semiconductor transition in germanium, *Phys. Rev. B* **49**, 14251 (1994).
- [38] John P. Perdew, Adrienn Ruzsinszky, Gábor I. Csonka, Oleg A. Vydrov, Gustavo E. Scuseria, Lucian A. Constantin, Xiaolan Zhou, and Kieron Burke, Restoring the Density-gradient Expansion for Exchange in Solids and Surfaces, *Phys. Rev. Lett.* **100**, 136406 (2008).
- [39] Jochen Heyd, Gustavo E. Scuseria, and Matthias Ernzerhof, Hybrid functionals based on a screened Coulomb potential, *J. Chem. Phys.* **118**, 8207 (2003).
- [40] Jochen Heyd, Gustavo E. Scuseria, and Matthias Ernzerhof, Erratum: Hybrid functionals based on a screened coulomb potential, *J. Chem. Phys.* **124**, 219906 (2006).
- [41] John P. Perdew, Kieron Burke, and Matthias Ernzerhof, Generalized Gradient Approximation Made Simple, *Phys. Rev. Lett.* **77**, 3865 (1996).
- [42] Hartwin Peelaers and Chris G. Van de Walle, Brillouin zone and band structure of  $\beta$ -Ga<sub>2</sub>O<sub>3</sub>, *Phys. Status Solidi B* **252**, 828 (2015).
- [43] Alex Zunger, S.-H. Wei, L. G. Ferreira, and James E. Bernard, Special Quasirandom Structures, *Phys. Rev. Lett.* **65**, 353 (1990).
- [44] A. van de Walle, P. Tiwary, M. De Jong, D. L. Olmsted, M. Asta, A. Dick, D. Shin, Y. Wang, L. Q. Chen, and Z. K. Liu, Efficient stochastic generation of special quasirandom structures, *Calphad Comput. Coupling Phase-Diagrams Thermochem.* **42**, 13 (2013).
- [45] Hartwin Peelaers, Daniel Steiauf, Joel B. Varley, Anderson Janotti, and Chris G. Van de Walle, (In<sub>x</sub>Ga<sub>1-x</sub>)<sub>2</sub>O<sub>3</sub> alloys for transparent electronics, *Phys. Rev. B* **92**, 085206 (2015).
- [46] See Supplemental Material at <http://link.aps.org/supplemental/10.1103/PhysRevApplied.10.011003> for further details on band-gap values, absolute positions of CBM and VBM, and corresponding bowing parameters.
- [47] Anderson Janotti and Chris G. Van de Walle, Absolute deformation potentials and band alignment of wurtzite ZnO, MgO, and CdO, *Phys. Rev. B* **75**, 121201 (2007).
- [48] Elena O. Filatova and Aleksei S. Konashuk, Interpretation of the changing the band gap of Al<sub>2</sub>O<sub>3</sub> depending on its crystalline form: Connection with different local symmetries, *J. Phys. Chem. C* **119**, 20755 (2015).